A&A 493, 613–621 (2009)
DOI: 10.1051/0004-6361:200810299

Astronomy & Astrophysics

Heights of solar tracers observed at 8 mm and an interpretation of their radiation

R. Brajša[1,⋆], I. Romštajn[2], H. Wöhl[3], A. O. Benz[4], M. Temmer[5], and D. Roša[2]

[1] Hvar Observatory, Faculty of Geodesy, University of Zagreb, Kačićeva 26, 10000 Zagreb, Croatia
e-mail: romanb@geof.hr
[2] Zagreb Astronomical Observatory, Opatička 22, 10000 Zagreb, Croatia
e-mail: ivan.romstajn@po.t-com.hr; drosa@zvjezdarnica.hr
[3] Kiepenheuer-Institut für Sonnenphysik, Schöneckstr. 6, 79104 Freiburg, Germany
e-mail: hw@kis.uni-freiburg.de
[4] Institute of Astronomy, ETH-Hönggerberg, HIT J 23.1, 8093 Zürich, Switzerland
e-mail: benz@astro.phys.ethz.ch
[5] Observatorium Kanzelhöhe/IGAM, Institut für Physik, Universität Graz, Universitätsplatz 5, 8010 Graz, Austria
e-mail: manuela.temmer@uni-graz.at

Received 31 May 2008 / Accepted 18 September 2008

ABSTRACT

Context. At the wavelength of 8 mm, emissive features (high brightness-temperatrue regions, HTRs) and absorptive features (low brightness-temperature regions, LTRs) can be traced for the determining the solar rotation. From earlier studies it is known that about two thirds of LTRs are associated with Hα filaments.
Aims. Thermal bremsstrahlung and gyromagnetic (cyclotron) radiation mechanism can be important for explaining the observed phenomena, so we determine the heights of solar structures and interpret their radiation mechanism(s).
Methods. We use the method of simultaneous determination of the solar synodic rotation velocity and the height of tracers. The rotation velocities were determined by the linear least-square fit of their central meridian distance as a function of time. We used a procedure for calculating the brightness temperature for a given wavelength and model atmosphere, which integrates the radiative transfer equation for the thermal bremsstrahlung.
Results. The mean value of the low brightness-temperature regions' heights is about 45 600 km. This height was used as input for constructing prominence and coronal condensation models, which, when assuming thermal bremsstrahlung as the radiation mechanism, yield a decrease in the brightness temperature of 2–14%, in agreement with observations. If the same radiation mechanism is considered, the models of the solar corona above active regions give an increase in the brightness temperature of 5–19%, also in agreement with observations. In this case an indirect indication (from the rotational analysis) that the HTRs are located higher in the solar atmosphere than the LTRs was taken into account.
Conclusions. The method for simultaneously determining the solar synodic rotation velocity and the height of tracers could have only been properly applied on LTRs, since a homogeneous distribution over latitudes and central meridian distances of a large enough data set is necessary. Thermal bremsstrahlung can explain both the LTR (prominences and coronal condensations) and HTR (ordinary active regions) phenomena observed at 8 mm. At this wavelength, thermal gyromagnetic emission is almost surely excluded as a possible radiation mechanism.

Key words. Sun: rotation – Sun: radio radiation – Sun: corona

1. Introduction

The heights of solar structures observed at wavelengths of about 1 cm are uncertain since the solar corona is mostly transparent in this wavelength range. The corresponding frequency of radiation is higher than the plasma frequency for altitudes over 200 km above the solar photosphere (e.g., Brajša 1993). Furthermore, various radiation mechanisms can be effective: besides thermal bremsstrahlung, gyromagnetic (cyclotron) radiation might also be important in the regions of strong magnetic fields (Aschwanden et al. 1995). In the quiet solar atmosphere, the optical depth $\tau = 1$ for thermal bremsstrahlung might already be reached at the height of about 2000 km (Schleicher 1976; Benz et al. 1997; Brajša et al. 2007b), so height determination of solar structures in this wavelenght range is important. The method of solar rotation stereoscopy developed by Aschwanden & Bastian (1994a,b) and Aschwanden et al. (1995) enables height determination at cm and mm wavelengths. In the present analysis, we use the method for the simultaneous determination of the solar synodic rotation velocity and the height of tracers developed by Roša et al. (1998). This method can be applied properly if the tracers used for determining the solar rotation are at least to some extent homogenously distributed over latitudes and central meridian distances. The structures' heights obtained in such a way are used then as constraints for modelling and interpreting the source radiation.

Special problem in solar rotation analysis using tracers at mm and cm wavelengths are the projection effects in the position determination, since the objects belong to the solar chromosphere and corona (e.g., Liu & Kundu 1976; Aschwanden et al. 1995; Brajša et al. 1997, 1999, 2000). If these effects are not taken into account, systematic influences on the solar-rotation

⋆ Alexander von Humboldt Research Fellow.

results (changes in the measured rotational velocity and heliographic latitude) may arise. This can make a comparison with rotational results misleading if obtained with photospheric tracers. To overcome that problem, a method was developed for simultaneously determining the solar synodic rotation velocity and the height of tracers (Roša et al. 1998). This method was later applied successfuly to Hα filaments (Vršnak et al. 1999) and to coronal bright points (Brajša et al. 2004). We note that projection effects can and must be corrected for coronal mass ejections (Vršnak et al. 2007) and the solar rotation determined by supergranules (Hathaway et al. 2006, and references therein).

The brightness temperature T_b is commonly used as a measure of radiation intensity in radio astronomy. On full-disc solar images obtained at mm and cm wavelengths, structures of lower and higher brightness temperatures than the quiet Sun level (qsl) can be distinguished. These are the low-temperature (LTRs, $T_b < T_{qsl}$) and high-temperature regions (HTRs, $T_b > T_{qsl}$), respectively. As tracers for solar rotation studies LTRs were often used (Brajša et al. 1992a, 1996, 1997, 1999, 2000, 2001), but also LTRs and HTRs (Liu & Kundu 1976; Urpo et al. 1989) and HTRs only (Teräsranta 1982; Urpo & Pohjolainen 1987; Aschwanden et al. 1995; Riehokainen et al. 1996, 1998). However, some of these studies were only based on limited data sets and the height correction was not always taken into account properly.

In the present work we use a series of diurnal full-disc solar maps recorded at the wavelength of 8 mm at the Metsähovi Radio Observatory in the years 1979–1982 and 1987–1991. The LTRs from that data set were analysed by Brajša et al. (1997). However, in that study a significant part of the LTR velocities was determined only approximatively by a graphic method, i.e., without a numerical calculation. In the present work we determine all rotation velocities in the same way by the calculation procedure described in Sect. 3.1. Furthermore, while some aspects of the LTRs' height correction were partially considered (Brajša et al. 1997, 1999, 2000), the whole method has not been consistently applied yet to the LTR data set, as in the present analysis (Sect. 3.2.). This enables us not only to correct the differential rotation profile obtained tracing LTRs, but also to determine the average heights of the used tracers. At these heights, various radiation sources will be modelled to understand which physical conditions can lead to the appearance of the LTR phenomena. Finally, we also include the rotational analysis of HTRs and an interpretation of their radiation.

In the Metsähovi maps, LTRs and HTRs were identified and traced. For the rotation analysis, only small, compact sources were used with substantially different brightness temperatures from the quiet Sun level. Large, diffuse LTRs with brightness temperatures just below the quiet Sun level were mostly excluded from the subsequent analysis. We note that in an earlier paper (Brajša et al. 1997, their Fig. 1), we analysed the number of LTRs according to the standard deviation of the mean LTR's latititude (for one subsample of the present data set). The maximum in the distribution lies between 1 and 2 deg of heliographic latitude, implying that the LTR minimum is a good measure of the position and consequently an appropriate tracer for the solar rotation determination.

2. Measurements and the data set

At the Metsähovi Radio Observatory, Helsinki University of Technology, solar observations have been performed with the 14 m dish radio telescope since 1976 (Urpo et al. 1994; http://kurp-www.hut.fi/sun/). The radio telescope can be used in the frequency range between 10 and 100 GHz, and diurnal full-disc solar maps taken at the frequency of 37 GHz (λ = 8 mm) were used in the present analysis. The beam width of the telescope amounts to 2.4 arcmin at this wavelength, and the quiet Sun level is estimated at a brightness temperature T_{qsl} = 7800 K (e.g., Urpo et al. 1994). The sensitivity of the receivers enables 0.1 s.f.u. resolution. On the temperature scale, this corresponds to a resolution of better than 100 K, and it is limited by short-term changes in the atmospheric attenuation (e.g., Urpo et al. 1994; Riehokainen et al. 1998; Pohjolainen et al. 2000).

Table 1. The number, n, of identified LTRs (HTRs) traced during d days.

LTRs:									
d	2	3	4	5	6	7	8	9	10
n	187	181	90	62	54	27	11	6	2
HTRs:									
d	2	3	4	5	6	7	8	9	10–13
n	21	28	24	21	22	20	8	3	8

Metsähovi full-disc solar maps at 8 mm can be visualized in various representations, such as maps with contours of constant brightness temperature (e.g., Urpo et al. 1989, 1994; Pohjolainen et al. 1991; Brajša et al. 1992b, 2007a), as grey-shadded plots (e.g., Brajša et al. 1996), and as colour maps where different colours represent different brightness temperatures (e.g., Brajša et al. 2007b). Several hundred full-disc solar contour maps recorded in the years 1979–1982 and 1987–1991 were analysed. In these maps the LTRs and HTRs were identified, with one example given in Fig. 1 in the paper by Brajša et al. (1992a).

The brightness temperature minima (maxima) inside the contours of LTRs (HTRs) were used as tracers for the solar rotation determination and their positions (the heliographic latitude and the central meridian distance, CMD) were determined. In the case of LTRs, small, compact objects having lowest brightness temperatures were identified and traced. Occasionally, multiple minima were found inside the same extended LTR areas, and treated as separate tracers. In the case of HTRs, the sources often had circular shapes, and geometrical midpoints were used as tracers' positions.

The accuracy of the heliographic coordinate determination was 1 deg, which is much better than the spatial resolution of the radio telescope. Estimating the uncertainty in the determination of solar coordinates to be 3–5 deg at medium latitudes and requiring a signal-to-noise ratio (S/N) better than 10, one finds that a feature should be traced at least 2 to 4 days, depending on the position on solar disc. Shorter tracing times, combined with the uncertainty mentioned in coordinate determination, could lead to unreliable results (Brajša et al. 1997). In total, 620 LTRs and 155 HTRs were identified and traced. The LTRs were followed in 2–10 consecutive maps and HTRs in 2–13 consecutive maps. In Table 1 we present the distribution of LTRs (HTRs) according to the tracing time expressed in days. From the table it can be seen that the tracing periods of 2 to 4 days were indeed the most common ones in the analysis of LTRs.

3. Methods of data reduction

3.1. The determination of the rotation velocity

The rotation velocities of LTRs and HTRs were determined by the linear least-square fit of their central meridian distance as a function of time, t. The transformation from the synodic to the

sidereal rotation velocity was performed using the constant factor ($\Delta\omega = 360\,\mathrm{deg}/365\,\mathrm{days}$), i.e., not as a season's dependent function, which is not needed because of the given precision of the position determination.

As usual, the solar differential rotation is represented by

$$\omega = A + B\sin^2\psi \tag{1}$$

where ω is the sidereal rotation velocity in deg/day, ψ the solar latitude in degrees, and A, B, the solar differential rotation parameters.

3.2. The method of the height correction

We now briefly describe the method of simultaneously determining of the solar rotation velocity corrected for projection and the height of tracers according to the paper by Roša et al. (1998). The main assumption of the method is the constant height of the tracers, which does not change significantly during the tracing. Furthermore, proper motions of the sources are supposed to be smaller than the spatial resolution of the radio telescope. Finally, unusually high rotation velocities, measured especially at large central meridian distances and high latitudes, are a consequence of projection effects, since it is certain that the tracers belong to the solar chromosphere and corona.

In the following the measured quantities are denoted with the asterisk (*) and the corrected ones without. First we introduce the parameter β, which connects the height parameter, $\epsilon = h/R$, where h is the height above the solar surface and R the solar radius, with the observed, ψ^*, and corrected, i.e., true latitude of the tracer, ψ,

$$\beta = (1+\epsilon)\frac{\cos\psi}{\cos\psi^*}\,. \tag{2}$$

This is Eq. (17b) in Roša et al. (1998), which can be approximated by

$$\beta = \frac{\sqrt{(1+\epsilon)^2 - \sin^2\psi^*}}{\cos\psi^*} = \mathrm{const.}, \tag{3}$$

for the case $B_0 \approx 0$, where B_0 is the heliographic latitude of the solar disc centre. This is Eq. (20b) in Roša et al. (1998). The relative deviation of the parameter β from a constant value due to the change of the projected heliographic latitude is less than 2% even in the most inconvenient cases when B_0 reaches the maximum value and the tracer is close to the limb (Roša et al. 1998).

Now we connect the parameter β with the mean observed CMD, λ^*, and corresponding observed, ω^*, and corrected rotation velocity, ω, of the measured tracer

$$\omega_i^* = \frac{\sqrt{\beta^2 - \sin^2\lambda_i^*}}{\cos\lambda_i^*}\omega. \tag{4}$$

This is Eq. (21d) in Roša et al. (1998).

Moreover, we introduce the following abbreviations

$$a = \sum_{i=1}^{N}\omega_i^{*2}, \tag{5}$$

$$b = \sum_{i=1}^{N}\frac{1}{\cos^4\lambda_i^*}, \tag{6}$$

$$c = \sum_{i=1}^{N}\frac{\omega_i^{*2}}{\cos^2\lambda_i^*}, \tag{7}$$

$$d = \sum_{i=1}^{N}\frac{1}{\cos^2\lambda_i^*}, \tag{8}$$

$$e = \sum_{i=1}^{N}\frac{N}{\cos^4\lambda_i^*}, \tag{9}$$

where the summation refers to 10-deg latitude bins and N is the number of measured pairs of velocity, ω_i^*, and mean CMD, λ_i^*, in each bin. The corrected rotation velocity ω and the parameter β can now be calculated by

$$\omega^2 = \frac{ab - cd}{e - d^2}, \tag{10}$$

$$\beta^2 = \frac{b - d + c/\omega^2}{b}, \tag{11}$$

which are Eqs. (33a) and (33b) in Roša et al. (1998), respectively.

Finally, the true height of the tracer is calculated by

$$h = R\left(\sqrt{\beta^2\cos^2\psi^* + \sin^2\psi^*} - 1\right), \tag{12}$$

where ψ^* is the mean latitude value for each latitude bin

$$\psi^* = \frac{1}{N}\sum_{i=i}^{N}\psi_i^*. \tag{13}$$

These two expressions are Eqs. (34) and (35) from Roša et al. (1998). Equations (12) and (3) hold in the approximation $B_0 \approx 0$. As already stressed, the relative deviation of the parameter β from a constant value due to the change of the projected heliographic latitude is less than 2% even in the most inconvenient cases when B_0 reaches the maximum value and the tracer is close to the limb (Roša et al. 1998). The mean value of the measured rotation velocities is calculated by

$$\omega^* = \frac{1}{N}\sum_{i=i}^{N}\omega_i^*, \tag{14}$$

for each latitude bin. The corrected latitude ψ is calculated by

$$\cos\psi = \frac{\beta\cos\psi^*}{\sqrt{\beta^2\cos^2\psi^* + \sin^2\psi^*}}\,. \tag{15}$$

This formula is obtained by combining Eqs. (2) and (3).

3.3. The determination of tracers' heights and corrected rotation velocities

This method relies on a homogeneous distribution of the measured rotation velocities according to the latitude and the CMD. The HTR data set is too small for a consistent and reliable application of the height correction. We can illustrate this by the fact that there were only 7 HTRs identified in the latitude band 30–40 deg and none of them at latitudes higher than 40 deg. Furthermore, in the CMD band 40–60 deg there were only 12 identified HTRs, so we continue only with the LTR data set.

Table 2. The number, n, of LTRs over latitudes (ψ) and central meridian distances (CMD).

ψ (deg)	0–10	10–20	20–30	30–40	40–50	50–60
n	554	250	278	291	118	27
CMD (deg)	0–10	10–20	20–30	30–40	40–50	50–60
n	451	431	341	217	74	4

The LTRs' tracing times were up to 10 days, and even after a few days, the CMD span is already too large, so that the observed rotation velocity cannot be properly connected with the corresponding mean CMD. For this reason, the whole LTR data set was reanalysed determining rotation velocitites with the method of daily shift, i.e., by dividing the observed CMD displacement with the elapsed time in pairs of consecutive images. In this way, after filtering out 124 unreasonably high or low rotation velocities, 1518 rotation values of LTRs (instead of 620 determined with the method described in Sect. 3.1.) were obtained, together with their corresponding latitudes and CMDs. The distributions of LTRs over latitudes and CMDs are presented in Table 2 for the data set of 1518 LTRs. North and south, as well as east and west are folded together. From the table it can be seen that both the latitudes and CMDs up to 50 deg are covered fairly well by LTRs, justifying the application of the method of the height correction for LTRs. After filtering out all sidereal rotation velocities less than 11.0 deg/day, 1365 values remained for further analysis. The upper limit of the rotation velocity filter was held open, since the extremely high-velocity values are considered as a consequence of projection effects.

The calculation of the height correction proceeds in the following way. All measured rotation velocities (after an application of the low filter only, as described above) with the corresponding mean values of the CMD are divided in 10-deg latitude bins. Both solar hemispheres were folded together. Now, for each latitude bin the mean value of the corrected rotation velocity ω and the parameter β are calculated according to Eqs. (10) and (11), respectively. The measured rotation velocities ω_i^* are then fitted as a function of the measured central meridian distance λ_i^* using Eq. (4) and taking into account the corrected ("true") rotation velocity ω and the value of the parameter β for each latitude bin.

Moreover, the height of the tracer above the solar surface (expressed in units of the solar radius R) is calculated by Eq. (12) for each latitude bin, taking the mean latitude into account of all measurements in each bin using Eq. (13). Finally, the corrected mean latitude for each bin is calculated by Eq. (15).

For each latitude bin, we now have the mean observed values of the latitude and the rotation velocity, ψ^* and ω^*, calculated using Eqs. (13) and (14), and the corresponding corrected values, ψ and ω calculated by Eqs. (10) and (15). From these values the corrections specific to each latitude bin are calculated as $\Delta\omega = \omega - \omega^*$ and $\Delta\psi = \psi - \psi^*$ and used to correct all individual measured pairs of the rotation velocity and latitude, for 620 rotation velocities of identified LTRs traced in 2 to 10 consecutive images. In this way the corrected data set of LTRs velocities was established.

4. Results

4.1. Solar differential rotation determined tracing low and high brightness temperature regions at 8 mm

We present the results on solar differential rotation for the three cases, HTRs without the height correction and LTRs without and with the height correction (Tables 3–5 and Fig. 1). The sidereal parameters from Eq. (1) and their standard errors (M) are expressed in deg/day. Both solar hemispheres are treated together and the number of tracers n is also given. To reject the statistically unreasonable velocity values due to possible false tracer identification and imprecise position determination, a running-average velocity filter over latitudes was applied (similar as in the rotational studies of coronal bright points, Brajša et al. 2002, and references therein). Extreme rotation velocity values were excluded in two steps, called filters in Table 3. (i) All sidereal rotation velocity values lower than 8 deg/day and higher than 18 deg/day were excluded regardless of the tracer's latitude. Then the rotation velocity parameters from Eq. (1) were found for all remaining data points (1st step). (ii) Next, a second filter excluding all velocity values differing by $\delta = 2.0$ deg/day or more from the mean curve was applied to the data and finally new parameters were calculated (2nd step). The solar differential rotation parameters after applying the 1st and the 2nd step filter are given in Tables 3–5, while in Fig. 1 the rotation profiles obtained only after the 2nd step filter are presented.

Table 3. Differential rotation parameters A and B for HTRs without the height correction.

A	$\pm M_A$	$-B$	$\pm M_B$	n	Remark
14.94	±0.15	3.18	±1.23	149	1st filter
14.91	±0.10	2.56	±0.84	141	2nd filter

Table 4. Similar to Table 3 for LTRs without the height correction.

A	$\pm M_A$	$-B$	$\pm M_B$	n	Remark
14.33	±0.09	1.89	±0.39	595	1st filter
14.44	±0.06	1.91	±0.26	494	2nd filter

Table 5. Similar to Table 4 for LTRs with the height correction.

A	$\pm M_A$	$-B$	$\pm M_B$	n	Remark
13.54	±0.13	2.09	±0.74	561	1st filter
13.92	±0.06	4.09	±0.34	462	2nd filter

Table 6. Effective heights of LTRs calculated for various latitude bins using Eqs. (12) and (13).

Latitude ψ (deg)	height h (km)	n	Remark
0–10	16 710	513	
10–20	55 918	227	
20–30	15 676	255	
30–40	58 109	252	
40–50	81 486	97	
50–60	−15 461	21	
		1365	total number
0–50	45 580		mean value
0–60	35 406		mean value

4.2. The heights of low temperature regions

The effective heights of LTRs are calculated for each 10-deg latitude bin using Eq. (12) and the results presented in Table 6. The numbers of used tracers in the latitude bins (n), the total number of tracers and the mean values of heights, with and without the results for the highest latutudes, are also given. According to the latitudinal distribution of LTRs, the first six

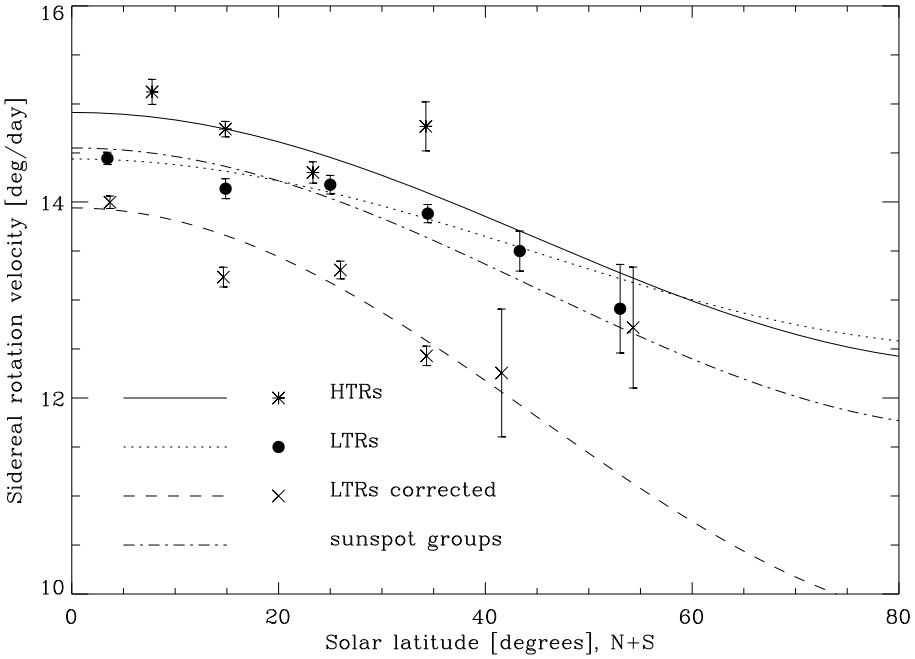

Fig. 1. The mean values of sidereal rotation velocities of HTRs and LTRs. For the LTRs, results with and without the height correction are presented, as indicated in the legend. The averaging is performed in 10-deg latitude bins and the error bars indicate the standard errors of the means in each bin (calculated as $M = \sigma/\sqrt{N}$, where σ is the standard deviation and N the number of data points in the bin). Both solar hemispheres are treated together and the lines represent least-square fits to Eq. (1) using all filtered data points for each case. For comparison, the differential rotation profile obtained tracing sunspot groups from the Greenwich data set (Balthasar et al. 1986) is also given.

latitude bands, i.e., latitudes up to 60 deg are taken into account. The calculated heights refer to the effective solar radius $R = R_0 + \Delta R = 696\,260$ km + 500 km = 696 760 km used in the coordinate transformation (Pohjolainen 2006). We obtained following heights of LTRs relative to the mentioned effective solar radius: $\bar{h} = (45\,580 \pm 12\,808)$ km for the latitudes in the range 0–50 deg and $\bar{h} = (35\,406 \pm 15\,283)$ km for the latitudes 0–60 deg. These effective heights were obtained by averaging the mean values for 5 and 6 latitude bins (Table 6), respectively. The standard errors are also given, expressed as $\sigma/\sqrt{N}$, where σ is the standard deviation and N the number of bins under consideration (Table 6). From further analysis we excluded the height derived in the last latitude band (50–60 deg). This result is unreliable due to the small number of data points at latitudes higher than 50 deg. In this latitude range (50–60 deg), only 27 LTRs were traced using the method of daily shift, as can be seen in Table 2. This is a relatively small number of tracers compared with the other 10-deg latitude bands where it varied between 118 and 554 (Table 2). The negative height obtained for this latitude band would indicate a tracer's height below the effective solar radius, which obviousy does not make sense. It is a consequence of the monotonically decreasing function ω(CMD) (three typical cases can be seen in Fig. 1b in the paper by Vršnak et al. 1999). In the present case, this function cannot be properly determined because the number of data points is too small in the latitude range under consideration.

5. An interpretation of low and high brightness-temperature region phenomena

5.1. Low-temperature regions

In one of our previous studies (Brajša et al. 1999), we found that two thirds (69%) of small, compact LTRs suitable for an analysis of the solar rotation were spatially associated with Hα filaments, i.e., prominences, in a qualitative agreement with other studies performed at the mm and cm wavelengths (Butz et al. 1976; Kundu et al. 1978; Schmahl et al. 1981; Kundu et al. 1986). These LTRs had brightness temperatures substantially lower than the quiet-Sun level and the association rate with Hα filaments was found to depend on the solar cycle phase, ranging from 39–76% (Brajša et al. 1999). It is interesting, that at shorter, submillimetre wavelengths, radio depressions associated with Hα filaments were also observed (Bastian et al. 1993), while at larger wavelengths of about 90 cm, the absorption is reversed to emission and Hα filaments are observed as HTRs (Lang 1989).

Free-free absorption (inverse bremsstrahlung) is the main radiation mechanism causing absorption, i.e., the radio depression and the LTR phenomenon at mm wavelengths associated with prominences. This process has been extensively studied (e.g., Chiuderi Drago 1990; Chiuderi & Chiuderi Drago 1991; Chiuderi Drago et al. 1992; Brajša 1993; Engvold 1994; Tapping & Harvey 1994; Bastian 1995), which is however not the case for LTRs not associated with prominences. We now develop models for both LTRs with and without associated prominences, calculate their brightness temperatures, and compare them with the observed values.

A quiet solar region having an average magnetic field less than 100 G emits radiation in the mm wavelength range by thermal bremsstrahlung in the temperature range between 10^4 K and 10^7 K (Hurford 1992) and this radiation mechanism is assumed here for the interpretation. In radio astronomy, intensities, I, are usually expressed in terms of the brightness temperature, T_b, using the Rayleigh-Jeans approximation of Planck's law

$$T_\mathrm{b} = \frac{c^2 I}{2\nu^2 k_\mathrm{B}}, \tag{16}$$

where ν is the observing frequency, k_B the Boltzmann constant, and c the speed of light. The brightness temperature is the solution of the radiative transfer equation

$$T_\mathrm{b} = \int_0^\infty T_\mathrm{e} \mathrm{e}^{-\tau} \mathrm{d}\tau, \tag{17}$$

where the optical depth, $\mathrm{d}\tau$, of bremsstrahlung for solar abundances neglecting the magnetic field is given by (e.g., Benz 2002):

$$\mathrm{d}\tau = \frac{0.01146 \ln\Lambda\, n_\mathrm{e}^2}{(1 - 8.06 \times 10^7 n_\mathrm{e}/\nu^2)^{1/2} \nu^2\, T_\mathrm{e}^{3/2}}\, \mathrm{d}s. \tag{18}$$

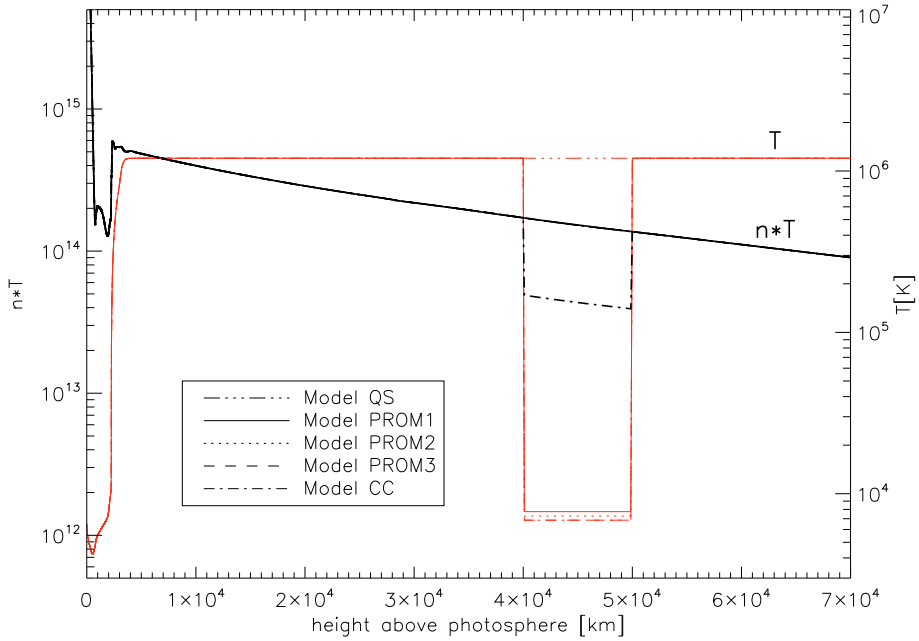

Fig. 2. The product (bold) of electron density n (cm^{-3}) and temperature T (K) as a function of height above the solar photosphere for the quiet Sun model (QS), various prominence models (PROM) and a model of the coronal condensation (CC), as indicated in the legend. Also, the temperature T (K) is overplotted for different models (with the temperature scale drawn on the right vertical axis).

The Gaunt factor, ln Λ, is a slowly varying function of the electron temperature, T_e, and density with a value of about 8 for the upper chromosphere.

Equations (17) and (18) indicate that the effect of a temperature increase on the radio intensity is model dependent. Our investigation is based on the models of Fontenla et al. (1993), describing average models that agree reasonably well with radio observations (Bastian et al. 1996). The average model is now disturbed to find the necessary deviations for the observed structures (LTRs and HTRs) at mm wavelength range.

The calculation was performed using a program that computes the brightness temperature for different wavelengths and stores the increase in brightness temperature per unit height in an array. Finally the program integrates these contributions and yields the total brightness temperature at each frequency.

Our starting model of the solar chromosphere and corona is the *FAL model A* (Fontenla et al. 1993), combined with the Baumbach-Allen coronal model at high altitudes using an electron temperature $T_e = 1.2\times10^6$ K (Benz et al. 1997). This model roughly describes the structure of a coronal hole (Brajša et al. 2007b), and we use it in the present analysis as a model of the quiet Sun (Model QS). We justify this assumption with our interest only in the relative deviation of the brightness temperature from some reference level, calculated for different models.

In the next step we construct deviations from the Model QS, taking into account the heights of LTRs obtained from the analysis of their differential rotation (Sect. 4.2). We change the temperature (T) and the density (n) in the height range from 40 000–50 000 km, representing the LTR body in the solar corona. For the interpretation, we consider prominences for LTRs associated with Hα filaments and coronal condensations for LTRs not associated with Hα filaments. According to Kundu et al. (1978) a coronal condensation, whose density is not high enough to be seen in Hα, can still cause absorption at mm wavelengths, i.e., lead to the appearance of an LTR.

Considering the typical physical parameters of prominences (e.g., Engvold et al. 1990) and coronal condensations (e.g., Kundu et al. 1978), we construct three prominence models (Models PROM1, PROM2, PROM3) and one model of the coronal condensation (Model CC). In the case of the three prominence models, we retain the hydrostatic equilibrium, multiplying the density n, by the same factor f, by which the temperature T is divided. In the case of the coronal condensation model, we keep the density lower than required by the equilibrium condition. It is about three times lower as for prominence models. In this case the pressure balance is kept by the magnetic field.

These five models are presented in Figs. 2 and 3. In Fig. 2 the product of electron density (n) and temperature (T) is given as a function of height above the solar photosphere. The pressure $p = nk_BT$ (where k_B is the Boltzmann constant) is exponentially decreasing in the corona at large scale. For the three PROM Models, there is no change in the pressure relative to the QS Model, while it is lower for the CC model. Figure 3 is similar to Fig. 2 , but only the density (n) is presented. In both cases (Figs. 2 and 3), the temperature (T) for all models is also overplotted.

The numerical parameters of the models and the calculated brightness temperatures are presented in Table 7. As can be seen in the table, the brightness temperature decreases for the three prominence models in the range from 100 K to 1000 K and for the coronal condensation model in the order of 1000 K. These values are in quantitative agreement with the observed brightness temperatures of LTRs measured at 8 mm (Pohjolainen et al. 1991; Brajša et al. 1992b; Brajša et al. 1997). However, we should bear in mind that the beam/convolution effect tends to decrease the amplitude of the brightness temperature depressions of small sources. In cases of large Hα filaments, the brightness temperature drop is up to 1000 K (an example is given in the paper by Vršnak et al. 1992), and in cases of smaller filaments, it can be less due the above-mentioned effect, i.e. in the range 100–1000 K. On the other hand, we note that our models can also interpret even lower brightness temperatures. For example, a prominence model with the temperature and density factor of 185 (see Table 7) yields a brightness temperature drop of about 1500 K, while its parameters are still within reasonable prominence values.

Concluding, we assume that thermal bremsstrahlung is the radiation mechanism, and by imposing physical conditions of prominences and coronal condensations at the heights derived

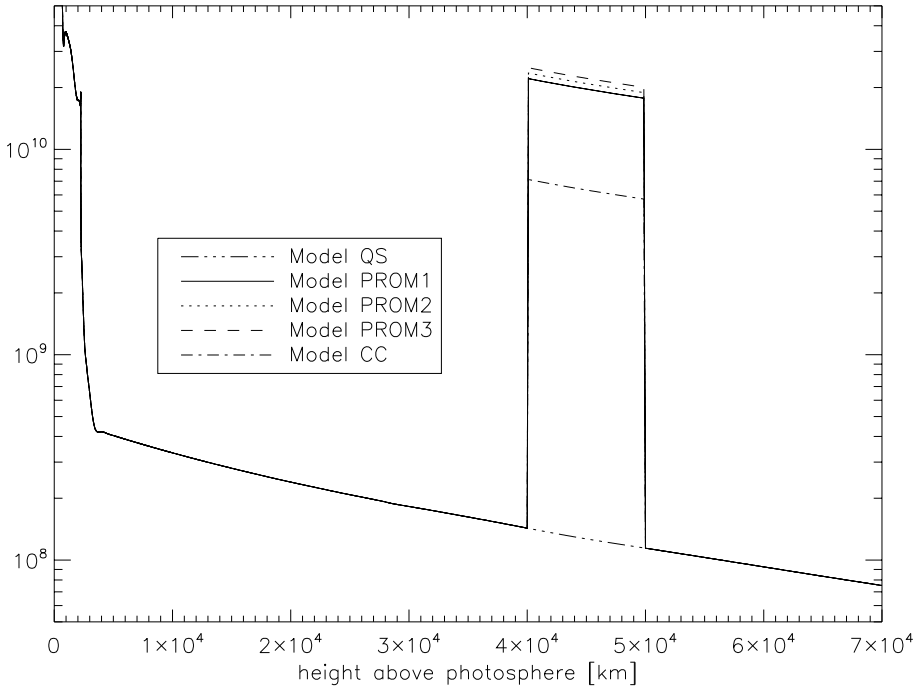

Fig. 3. Similar to Fig. 2 for the density.

Table 7. Temperature (T), density (n), and resulting brightness temperature (T_b) for the five models.

Model	Temperature	T (K)	Density	n (cm^{-3})	Brightness temperature T_b (K)	$-\Delta T_b$ (K)	$-\Delta T_b$ (%)
Model QS	T_{QS} =	1.2×10^6	n_{QS} =	1.286×10^8	7841		
Model PROM1	$T_{QS}/155$ =	7742	$n_{QS}\times155$ =	1.993×10^{10}	7701	140	1.8
Model PROM2	$T_{QS}/165$ =	7273	$n_{QS}\times165$ =	2.122×10^{10}	7216	625	8.0
Model PROM3	$T_{QS}/175$ =	6857	$n_{QS}\times175$ =	2.251×10^{10}	6779	1062	13.5
Model CC	$T_{QS}/175$ =	6857	$n_{QS}\times50$ =	6.430×10^9	6882	959	12.2

from the analysis of differential rotation, we can explain both the LTRs with and without associated filaments.

5.2. High-temperature regions

In the case of HTRs, which are mostly related to ordinary active regions, two mechanisms may be important. If thermal bremsstrahlung is considered as the radiation mechanism, then the enhanced intensity is a consequence of the increased density in the optically thin corona. The other radiation mechanism is gyromagnetic (cyclotron) emission from areas with strong magnetic field (e.g. Aschwanden et al. 1995). Such areas are expected to be located in ordinary active regions.

Concerning thermal bremsstrahlung, we construct different models, as in the case of LTRs (previous subsection). We assume that, above active regions, the solar atmosphere has a disturbed temperature and density structure in the range of heights 10 000–80 000 km. In all three cases, the coronal temperature is increased by a factor of 2 and the density by factors of 5, 7, and 10, for the models AR1, AR2, and AR3, respectively. These conditions are summarised in Table 8, where the resulting brightness temperatures are also given, while the densities at some characteristic heights for these three models are given in Table 9. The brightness temperature of HTRs modelled in such a way is enhanced by 5–20% (Table 8), in agreement with observations (e.g., Pohjolainen et al. 1991). Finally we note that, in our models, an increase of the coronal temperature, while keeping the same density structure, decreases the resulting brightness temperature, as expected for that temperature range.

6. Discussion and conclusions

In the present work, we have simultaneously determined the solar synodic rotation velocity and the height of tracers. This method can be properly applied only if there are enough rotation velocity measurements provided by observations, which are distributed reasonably well over solar latitudes and central meridian distances. This was the case only with LTRs in our data set. As a consequence of the height correction, the solar differential rotation curve was shifted to the systematically lower values, and the profile also became more differential (Fig. 1, Tables 4 and 5).

This method also enables the determination of the tracers' heights. The mean value of the LTR' heights was found to be about 45 600 km (Table 6). This result was than used to model prominences and coronal condensations (Figs. 2 and 3, Table 7). Assuming thermal bremsstrahlung as a radiation mechanism, the observed brightness temperatures of LTRs associated with Hα filaments (solar prominences) and of LTRs not associatied with Hα filaments (coronal condensations) can be successfully reproduced (Table 7).

In the case of HTRs, the method described above could not be applied, but systematically higher rotation velocities of HTRs than of LTRs at low latitudes (Fig. 1) represent an indirect indication that the HTRs have higher altitudes than the LTRs (as discussed by Adams & Tang 1977; by Aschwanden et al. 1995; and by Brajša et al. 1999, for various tracers). The differential rotation profile of sunspot groups was overplotted in Fig. 1 for comparison. We note that the slope of the differential rotation curve of HTRs is very similar to that of sunspot groups,

Table 8. Temperature (T), density (n) and resulting brightness temperature (T_b) for the four models under consideration.

Model	Temperature	T (K)	Density n	Brightness temperature T_b (K)	$+\Delta T_b$ (K)	$+\Delta T_b$ (%)
Model QS	T_{QS} =	1.2×10^6	n_{QS}	7841		
Model AR1	$T_{QS} \times 2$ =	2.4×10^6	$n_{QS} \times 5$	8201	360	4.6
Model AR2	$T_{QS} \times 2$ =	2.4×10^6	$n_{QS} \times 7$	8565	724	9.2
Model AR3	$T_{QS} \times 2$ =	2.4×10^6	$n_{QS} \times 10$	9338	1497	19.1

Table 9. Density (n) at given heights (h) for the four models given in Table 8.

Height h (km)	Density n (cm^{-3}) QS Model	AR1 Model	AR2 Model	AR3 Model
10 000	3.327×10^8	1.664×10^9	2.329×10^9	3.327×10^9
20 000	2.397×10^8	1.199×10^9	1.678×10^9	2.397×10^9
30 000	1.823×10^8	9.115×10^8	1.276×10^9	1.823×10^9
40 000	1.430×10^8	7.150×10^8	1.001×10^9	1.430×10^9
50 000	1.142×10^8	5.710×10^8	7.994×10^8	1.142×10^9
70 000	7.517×10^7	3.759×10^8	5.262×10^8	7.517×10^8

suggesting that both tracers are related to ordinary active regions. However, the HTR curve is systematically shifted to higher values. This shift is consistent with the uncorrected heights of HTRs due to projection effects, as earlier discussed. Using this information and again assuming thermal bremsstrahlung as the radiation mechanism, we have also successfully modelled HTRs (Tables 8 and 9).

As an alternative, we consider the case of thermal gyromagnetic radiation for HTRs. The emission is caused by non-relativistic electrons spiralling in the magnetic field and is also termed cyclotron radiation. The gyromagnetic absorption coefficient, κ, has a maximum at the harmonics $\nu = s\nu_B$

$$\kappa(\nu) = \frac{(2\pi)}{c} \frac{\nu_p^2}{\nu} \frac{\frac{(s/2)^{2s}}{s!} \sin\theta^{2s-2}(1+\cos\theta)}{\cos\theta} \beta_0^{2s-3} \qquad (19)$$

(from Melrose 1985), where ν is the observing frequency, $\nu_p = (n_e e^2/(\pi m_e))^{1/2}$ is the plasma frequency, n_e the electron density, m_e the electron mass, s the harmonic number, θ the angle between the magnetic field and the line of sight, $\beta_0 = (2kT/(m_e c^2))^{1/2}$, and $\nu_B = eB/(2\pi m_e c)$ is the electron gyrofrequency. From the models (Table 9) we take $T \approx 2.4 \times 10^6$ K, $n_e \approx 2 \times 10^8$ cm^{-3}. Thus $\nu_p \approx 127$ MHz and $\beta_0 \approx 0.02844$.

The resonance length is $l = 2\Lambda_B \beta_0 \cos\theta$, where Λ_B is the magnetic scale length, which we assume to be approximately 10^4 km. Thus $l \approx 2.84 \times 10^7$ cm. The optical thickness $\tau = \kappa l$. To contribute to the thermal emission, τ must reach a value of at least a tenth of a percent.

The observing frequency of 37 GHz would require a magnetic field of 6600 Gauss for resonance at the harmonic $s = 2$. Such a field has never been reported for the Sun. Thus we exclude the second harmonic. At the higher harmonics, τ becomes 0.402, 1.37×10^{-3}, 6.16×10^{-6} for $s = 3$, 4, and 5, respectively. The third and fourth harmonics could contribute significantly. This would require a magnetic field of 4400 Gauss or 3300 Gauss, respectively. These values are highly unlikely at the heights where the HTRs are observed. At the harmonics $s \geq 4$, the contribution of gyromagnetic radiation becomes negligible at our observing frequency and for our models.

We conclude that thermal bremsstrahlung can explain both the emission (HTRs) and absorption (LTRs) phenomena at the wavelength of 8 mm (corresponding to the frequency of 37 GHz). However, our interpretation of the HTR emission by thermal bremsstrahlung does not exclude thermal gyromagnetic emission at lower frequencies (e.g. Aschwanden et al. 1995).

Acknowledgements. R.B. gratefully acknowledges the support by the Deutsche Forschungsgemeinschaft, Bonn (project WO 191/11-1), and by the ETH, Zurich, partially supported by the Swiss National Science Foundation (200020-121676). M.T. gratefully acknowledges the Austrian Academy of Sciences (APART-11262) for support. Also, the support from the Austrian-Croatian Bilateral Scientific Project is acknowledged. The authors would like to thank Dr. Silja Pohjolainen for measuring the positions of objects in Metsähovi maps obtained at 8 mm, Dr. Bojan Vršnak for stimulating discussions and the anonymous referee for helpful comments and suggestions.

References

Adams, W. M., & Tang, F. 1977, Sol. Phys., 55, 499
Aschwanden, M. J., & Bastian, T. S. 1994a, ApJ, 426, 425
Aschwanden, M. J., & Bastian, T. S. 1994b, ApJ, 426, 434
Aschwanden, M. J., Lim, J., Gary, D. E., & Klimchuk, J. A. 1995, ApJ, 454, 512
Balthasar, H., Vázquez, M., & Wöhl, H. 1986, A&A, 155, 87
Bastian, T. S. 1995, in Infrared Tools for Solar Astrophysics: What's Next?, Proc. 15th NSO/SP Summer Workshop, ed. J. R. Kuhn & M. J. Penn (Singapore: World Scientific), 115
Bastian, T. S., Ewell, M. W., & Zirin, H. 1993, ApJ, 418, 510
Bastian, T. S., Dulk, G. A., & Leblanc, Y. 1996, ApJ, 473, 539
Benz, A. O. 2002, Plasma Astrophysics, 2nd edn. (Dordrecht: Kluwer Academic Publishers)
Benz, A. O., Krucker, S., Acton, L. W., & Bastian, T. S. 1997, A&A, 320, 993
Brajša, R. 1993, Sol. Phys., 144, 199
Brajša, R., Ruždjak, V., Vršnak, B., et al. 1992a, in The Solar Cycle, ed. K. L. Harvey, ASP Conf. Ser., 27, 274
Brajša, R., Vršnak, B., Ruždjak, V., et al. 1992b, Hvar Obs. Bull., 16, 1
Brajša, R., Ruždjak, V., Vršnak, B., et al. 1996, Hvar Obs. Bull., 20, 15
Brajša, R., Ruždjak, V., Vršnak, B., et al. 1997, Sol. Phys., 171, 1
Brajša, R., Ruždjak, V., Vršnak, B., et al. 1999, Sol. Phys., 184, 281
Brajša, R., Ruždjak, V., Vršnak, B., et al. 2000, Sol. Phys., 196, 279
Brajša, R., Ruždjak, V., Vršnak, B., et al. 2001, in The Dynamic Sun, eds. A. Hanslmeier, et al. (Dordrecht: Kluwer Academic Publishers), ASSL, 259, 263
Brajša, R., Wöhl, H., Vršnak, B., et al. 2002, A&A, 392, 329
Brajša, R., Wöhl, H., Vršnak, B., et al. 2004, A&A, 414, 707
Brajša, R., Benz, A. O., Temmer, M., et al. 2007a, Cent. Eur. Astrophys. Bull., 31, 219
Brajša, R., Benz, A. O., Temmer, M., et al. 2007b, Sol. Phys., 245, 167
Butz, M., Hirth, W., & First, E. 1976, Mitt. Astron. Ges., 38, 211
Chiuderi Drago, F. 1990, in Dynamics of Quiescent Prominences, ed. V. Ruždjak, & E. Tandberg-Hansen, Lecture Notes in Phys., 363, IAU Coll., 117, 70
Chiuderi, C., & Chiuderi Drago, F. 1991, Sol. Phys., 132, 81
Chiuderi Drago, F., Engvold, O., & Jensen, E. 1992, Sol. Phys., 139, 47

Engvold, O. 1994, in Solar Coronal Structures, ed. V. Rušin et al. (Bratislava: VEDA Publ.) Comp., IAU Coll., 144, 297
Engvold, O., Hirayama, T., Leroy, J. L., Priest, E. R., & Tandberg-Hanssen, E. 1990, in Dynamics of Quiescent Prominences, ed. V. Ruždjak, & E. Tandberg-Hansen, Lecture Notes in Phys., 363, IAU Coll., 117, 294
Fontenla, J. M., Avrett, E. H., & Loeser, R. 1993, ApJ, 406, 319
Hathaway, D. H., Williams, P. E., & Cuntz, M. 2006, ApJ, 644, 598
Hurford, G. J. 1992, in The Sun: A Laboratory for Astrophysics, ed. J. T. Schmelz & J. C. Brown, NATO (Dordrecht: Kluwer Academic Publishers), ASI Ser., 373, 297
Kundu, M. R., Fürst, E., Hirth, W., & Butz, M. 1978, A&A, 62, 431
Kundu, M. R., Melozzi, M., & Shevgaonkar, R. K. 1986, A&A, 167, 166
Lang, K. R. 1989, Hvar Obs. Bull., 13, 93
Liu, S.-Y., & Kundu, M. R. 1976, Sol. Phys., 46, 15
Melrose, D. B. 1985, in Solar Radiophysics, ed. D. J. McLean & N. R. Labrum, (Cambridge: Cambridge University Press), 220
Pohjolainen, S. 2006, private communication
Pohjolainen, S., Urpo, S., Teräsranta, H., et al. 1991, Hvar Obs. Bull., 15, 21
Pohjolainen, S., Portier-Fozzani, F., & Ragaigne, D. 2000, A&AS, 143, 227
Riehokainen, A., Urpo, S., & Valtaoja, E. 1996, Helsinki University of Technology, Metsähovi Radio Research Station, Ser. A, Report 22
Riehokainen, A., Urpo, S., & Valtaoja, E. 1998, A&A, 333, 741
Roša, D., Vršnak, B., Božić, H., et al. 1998, Sol. Phys., 179, 237
Schleicher, H. 1976, Ph.D. Thesis, Univ. Göttingen, 208
Schmahl, E. J., Bobrowsky, M., & Kundu, M. R. 1981, Sol. Phys., 71, 311
Tapping, K. F., & Harvey, K. L. 1994, in The Sun as a Variable Star, ed. J. M. Pap et al. (Cambridge Univ. Press), IAU Coll., 143, 182
Teräsranta, H. 1982, in Proc. XVI Finnish Astronomers' Days, ed. S. Urpo, Helsinki Univ. of Technology, Radio Lab., Report S 129, 29
Urpo, S., & Pohjolainen, S. 1987, Hvar Obs. Bull., 11, 137
Urpo, S., Pohjolainen, S., Teräsranta, H., et al. 1989, Hvar Obs. Bull., 13, 437
Urpo, S., Pohjolainen, S., & Teräsranta, H. 1994, Solar Observations at Metsähovi in 1993, Helsinki Univ. of Technology, Metsähovi Radio Research Station, Series A, Report 16
Vršnak, B., Pohjolainen, S., Urpo, S., et al. 1992, Sol. Phys., 137, 67
Vršnak, B., Roša, D., Božić, H., et al. 1999, Sol. Phys., 185, 207
Vršnak, B., Sudar, D., Ruždjak, D., & Žic, T. 2007, A&A, 469, 339